## **RESEARCH PAPER**

# Synthesis and Ameliorating the Morphological, Structural and Linear/Nonlinear Optical Features of PVA/SnO<sub>2</sub>-SiC Nanostructures for Optoelectronics and Radiation Shielding Applications

Ali Hussein Kareem \*, Majeed Ali Habeeb

Department of Physics, College of Education for Pure Sciences, University of Babylon, Iraq

#### ARTICLE INFO

## Article History: Received 05 June 2025 Accepted 27 September 2025 Published 01 October 2025

#### Keywords:

Antibacterial activity
Linear/nonlinear optical
properties
Radiation attenuation\
SnO<sub>2</sub>-SiC nanoparticles
Structural properties

## **ABSTRACT**

Owing to their potent antibacterial properties and nanoscale dimensions, nanoparticles have emerged as a viable alternative for various medical and technological applications. This research involved fabricating polymer nanocomposite samples via the solution casting method. The test samples used polyvinyl alcohol (PVA) polymer as the host matrix. Different concentrations of tin dioxide (SnO<sub>2</sub>) and silicon carbide (SiC) nanoparticles were introduced into the samples at various weight ratios (0%, 2%, 4%, 6%, and 8%) wt.%. The (PVA/SnO<sub>2</sub>-SiC) nanostructures demonstrate exceptional characteristics, including cost-effectiveness, advantageous optical properties, and reduced weight relative to other nanosystems. This study investigated the structural, optical (linear/ nonlinear), morphological and radiation attenuation properties of the (PVA/SnO<sub>3</sub>-SiC) nanostructures. It was discovered that polyvinyl alcohol (PVA) is amorphous, and with the increase of (SnO<sub>2</sub>-SiC) nanoparticles in the polymer samples, the rate of crystallite increases through (XRD). The microstructure of the materials was characterized, and the elements of the (SnO<sub>2</sub>-SiC) nanoparticles were detected through (EDS). Optical microscope pictures revealed that the nanoparticle dispersion within the mixture had a homogenous pattern, creating a coherent network throughout the polymer matrix. The experimental findings on the optical characteristics of (PVA/SnO2-SiC) nanocomposites indicated that the recorded absorption values, absorption coefficient (a), extinction coefficient (k), refractive index (n), real  $(\epsilon_{_1})$  and imaginary  $(\epsilon_{_2})$  dielectric constants, and optical conductivity  $(\sigma_{_{op}}),$  dispersion factors, nonlinear refractive index  $(n_2)$ , linear susceptibility  $(\chi^{(1)})$ , Urbach tail energy  $(E_u)$ , nonlinear susceptibility ( $\chi^{(3)}$ ), average oscillator coefficient ( $\lambda_0$ ),  $n_0$ , which stands for zero-frequency refractive index, and  $\varepsilon_0$ , which stands for zerofrequency dielectric constant of pure polyvinyl alcohol (PVA) increased with higher concentrations of (SnO<sub>2</sub>-SiC) nanoparticles.

## How to cite this article

Kareem A., Habeeb M. Synthesis and Ameliorating the Morphological, Structural and Linear/Nonlinear Optical Features of PVA/SnO<sub>2</sub>-SiC Nanostructures for Optoelectronics and Radiation Shielding Applications. J Nanostruct, 2025; 15(4):2411-2429. DOI: 10.22052/JNS.2025.04.078

<sup>\*</sup> Corresponding Author Email: ali.h.kareem.88@gmail.com

#### INTRODUCTION

Sophisticated composite materials have been increasingly employed in the marine, aerospace, and automotive industries since the 1960s as a result of their exceptional engineering properties, including reduced density, excellent fatigue resistance, high specific strength, high damping capacity, stiffness, and low thermal expansion coefficient. Polymer insulators are employed in various applications, including printed circuit boards, corrosion-resistant electronics, cable sheathing materials, and wire encapsulation. Polymers provide numerous benefits, including ease of processing, superior strength, outstanding flexibility and mechanical properties, and cost efficiency [1]. Unlike its bigger bulk counterparts, nanotechnology is an emerging field in the 21st century defined by nanoparticles that exhibit distinctive optical, magnetic, structural, mechanical, and electrical capabilities due to their nanoscale size ranging from (1 - 100 nm) [2]. Therefore, Nanotechnology has experienced a surge in popularity in recent years. According to research on matrix materials, nanocomposites are classified into three specific varieties: polymer matrix nanocomposites PMNC, metal matrix nanocomposites MMNC, and ceramic matrix nanocomposites CMNC [3]. Nanocomposites are defined as composite materials that incorporate at least one component at the nanometric scale (10-9 m) [4]. Synthetic and natural polymers as well as nanomaterials—defined as materials having a nanoscale structure or made up of nanoscale components—make up nanocomposites. They may also include a polymer matrix that uniformly incorporates various nanofillers. Nanocomposites (NCs) comprising nanoparticles (NPs) and polymers exhibit significant performance enhancements at substantially lower loadings compared to pure polymers [5,6]. The primary objective is to integrate the exceptional material characteristics the nanofillers with straightforward manufacturing processes of polymers, resulting in composite materials that demonstrate markedly enhanced macroscopic properties. The reduction of fillers to nanoscale dimensions leads to the phenomena observation of unique nanocomposites, which significantly enhances the interaction between fillers and polymers [7]. Nanoparticles possess distinct features that render them highly versatile for many applications. Nanoparticles exhibit size, shape, and dimension

variations alongside their inherent material properties and exhibit different physical, chemical, and biological features than their larger counterparts [8]. Polymer nanocomposites have garnered more attention from researchers and engineers owing to the superior performance of the matrix. Consequently, it is implemented to alter the structure and enhance the properties of the materials, leading to a significant improvement in the properties of the polymers and materials due to the influence of the nanoparticle [9]. Polymer nanocomposites warrant increased attention due to their superior efficacy, which is ascribed to the impact of nanofillers on the mechanical structure and other features. Nonetheless, the nanofillers possess a lower weight and necessitate reduced reinforcing compared to other matrix constituents. Interest in metal oxide nanoparticles has significantly increased, largely because of their extensive use as catalysts in various industries, antimicrobial agents, applications in medicine, fillers, chemical sensors, disinfectants, semiconductors, and their cosmetics significant impact on and microelectronics [10]. Globally, nanotechnology has steadily and firmly infiltrated various industries. The swift pace of technological progress is particularly evident in the manufacturing world, where nanoscale emporiums have expanded over the past decade. The rapid advancement of nanoscience that suggests nanoscale manufacturing will shortly be included in almost every technology discipline [11]. Silicon carbide (SiC) is a non-oxide ceramic semiconductor material characterized by numerous outstanding properties, including high thermal conductivity, resistance to reactions with acids and solvents, exceptional oxidation resistance, remarkable thermal shock resistance, and extremely high hardness. These attributes contribute to its extensive application in microwave electrical insulators and energy storage materials [12,13]. Since 1893, silicon carbide powder has been manufactured for its application as an abrasive. The presence of abrasive zones inside a metal work piece leads to rapid tool wear, increases cutting force, and greatly affects the quality of the conical surface [14]. Silicon carbide grains can be bonded together through roasting to create exceptionally hard ceramics, making it highly suitable for applications that demand high tolerances, including automobile brakes, ceramic

plates, bulletproof vests, high-speed steel polishing processes, deep drawing dies, and carbide inserts [15]. Silicon carbide technology has advanced significantly due to its distinct properties, resulting in the development of new devices. In addition to its established use as a bulk material, SiC is also investigated as a filler in polymer matrices to create composite materials aimed at enhancing specific properties. Silicon carbide exhibits enhanced wear resistance and mechanical strength. Because of its exceptional electrical and optical characteristics, tin oxide (SnO<sub>3</sub>), a transparent conducting oxide, has garnered much interest as a nanostructured material. With a band gap of around 3.68 electron volts (eV), the material shows a significant energy difference between its valence and conduction bands. It has a considerable n-type conductivity and a 130 meV exciton binding energy under ambient circumstances. This material may be used in gas sensing and biomedical applications because of its non-toxic properties, chemical sensitivity, thermal stability, and affordability [9]. SnO<sub>3</sub> has considerable promise as a material for several applications, including photocatalysis, solar cells, and novel optoelectronic devices. Owing to its elevated transmittance in the visible spectrum and a characteristic conductivity of 102-103 ( $\Omega$  cm)<sup>-1</sup> [16]. Polymers have become ubiquitous in our daily lives due to their indispensable role in providing essential services, making it difficult to imagine a viable existence without them [17]. The many advantageous qualities of polyvinyl alcohol (PVA) as a host matrix for metal oxide nanofillers include biodegradability, lack of toxicity, film-forming ability, ease of processing, transparency, low refractive index, and great mechanical capabilities. It also has minimum light scattering and minor imperfections [18]. PVA is a water-soluble synthetic polymer that is an odorless, tasteless, transparent, white or cream-colored granular powder. The material's diverse physical properties make it suitable for many practical applications. One of the beneficial properties of polyvinyl acetate (PVA) is its resistance to the harmful effects of solvents and oils and its strong adhesion to cellulose-based materials. Hence, the antioxidant is widely used in the paper, textile, and film industries [19]. Polyvinyl alcohol (PVA) has remarkable mechanical properties such as high tensile strength and flexibility, integration with biological processes, harmless semi-crystalline structure, durable

reliability as an organic material, ability to form homogeneous films, resistance to temperatures, and excellent barrier properties against oxygen and odor. In addition, it possesses commendable properties in terms of film formation, mixing, and adhesion. The visible light transmission exhibits remarkable strength. The importance of PVA polymer composites in scientific applications has been widely recognized [20]. The attainment of gamma radiation shielding is an important area of focus when considering external exposure due to its remarkable ability to penetrate deeply into the material and its potential adverse effects on human health. Prioritizing shielding is vital for protecting personnel and equipment due to the increasing use of radioactive materials in medicine and industry [21]. This study presents a cost-effective and straightforward method (PVA/SnO<sub>2</sub>-SiC) synthesis of nanostructures, emphasizing their potential applications in optoelectronics and gamma radiation shielding. The reasoning for undertaking this work stems from the growing global interest in ternary nanocomposites, which offer the potential to enhance material properties via a polymer matrix. The aim of this study is to create a novel (PVA/SnO<sub>2</sub>-SiC) nanocomposite material using the solution cast technique, intended for applications in optoelectronics, antibacterial properties, and gamma-ray shielding.

### **MATERIALS AND METHODS**

Films composed of nanocomposites were created using the casting method, integrating polyvinyl alcohol (PVA), tin dioxide (SnO<sub>2</sub>) nanoparticles, and silicon carbide (SiC). The experimental protocol involved dissolving pristine polyvinyl alcohol (PVA) in 30 ml of distilled water for a period of 40 minutes. Stir the mixture magnetically at 65 °C to ensure a consistent solution throughout. The polymer underwent modification by integrating tin dioxide (SnO<sub>2</sub>) and silicon carbide (SiC) nanoparticles at varying weight percentages: 2%, 4%, 6%, and 8%. After five days of natural evaporation in ambient conditions, the successful formation of polymer nanocomposites was observed. The PVA/SnO<sub>2</sub>-SiC nanocomposites were carefully extracted from the Petri plate and employed for measurement purposes. Fourier Transform Infrared Spectroscopy investigates nanocomposite samples of (PVA/ SnO<sub>3</sub>-SiC) within the wavenumber range of (500–

4000) cm<sup>-1</sup>. The samples underwent evaluation at different concentrations utilizing an Olympustype Nikon-73346 optical microscope, featuring a magnification of 10X and equipped with a camera for capturing microscopic images. Furthermore, X-ray diffraction (XRD) measurements along with surface morphology analysis were performed utilizing a field emission scanning electron microscope (FE-SEM) (Hitachi SU6600) and energydispersive X-ray spectroscopy (EDS). Employing nanocomposites for the purpose of gamma-ray attenuation. The samples were arranged in front of a concentrated beam generated by gammaray sources, particularly Cs-137, exhibiting an activity of 5 mCi. The separation between the gamma-ray source and the detector measures 2 cm. The linear attenuation coefficients were assessed using Geiger counter measurements to analyze the transmitted gamma-ray fluxes through nanocomposites composed of (PVA/SnO<sub>2</sub>-SiC)

Absorbance, absorption, and transmittance coefficients are determined using the following equations [22].

$$A = \frac{I_o}{I_A} \tag{1}$$

$$T_{r} = \frac{I_{T_{r}}}{I_{o}} \tag{2}$$

$$\alpha = \frac{(2.303 \times A)}{d} \tag{3}$$

Where A signifies absorption,  $I_{\rm Tr}$  indicates the intensity of transmitted light,  $I_{\rm 0}$  denotes the intensity of incident light, d refers to sample thickness, and  $I_{\rm A}$  represents the intensity of absorbed light.

The relation between the Urbach tail energy  $E_u$  and absorption coefficient  $\alpha$  is expressed as [23].

$$\alpha h \upsilon = B(h \upsilon - E_g)^r \tag{4}$$

hu, B, E<sub>g</sub>, and r depict photon energy, constant, energy band gap, and forbidden (r=3), allowed (r=2) indirect transitions, respectively.

equation was used to get the extinction coefficient (k) [24].

$$k = \frac{\alpha \lambda}{4\pi} \tag{5}$$

The wavelength is indicated by  $(\lambda)$ , while the absorption coefficient is written as  $(\alpha)$ . Determined the refractive index (n) using the formula [25].

$$n = \sqrt{4R - \frac{k2}{(R-1)2} - \frac{(R+1)}{(R-1)}}$$
 (6)

The reflection is represented as (R), and the reflectivity values used in refractive index formula no. 5 were obtained from the subsequent relationship:

$$R + T + A = 1 \tag{7}$$

The dielectric constant is comprised of two distinct components: the real portion, denoted as  $\varepsilon_1$ , and the imaginary part, represented as  $\varepsilon_2$ . The subsequent formulas may be employed to derive both the real and imaginary components [26].

$$\varepsilon_1 = n^2 - k^2 \tag{8}$$

$$\varepsilon_2 = 2nk \tag{9}$$

The optical conductivity  $(\sigma_{op})$  can be calculated using the following formula [27].

$$\sigma_{\rm op} = \alpha nc/4\pi \tag{10}$$

Where: c is the velocity of light

The relation between the Urbach tail energy  $E_{\mu}$  and absorption coefficient  $\alpha$  is expressed as [28].

$$\alpha = \alpha_0 e^{hv/Eu} \tag{11}$$

Wemple and Di-Domenico propose a single effective oscillator model that can correctly characterize the relationship between the photon energy and index of refraction [29].

$$\frac{1}{(n^2 - 1)} = \frac{E_{ose}}{E_d} - \frac{(hv)^2}{E_d E_{osc}}$$
 (12)

 $\rm E_{\rm d}$  denotes the dispersion energy, and  $\rm E_{\rm osc}$  represents a single oscillator's energy.

Furthermore, the comprehension of  $E_{osc}$  and  $E_{d}$  may be used to determine the zero-frequency refractive index  $n_{o}$  and the zero-frequency dielectric constant  $\epsilon_{o}$  through the relationship [30].

$$\varepsilon_{\rm o} = n_{\rm o}^2 = 1 + \frac{E_{\rm d}}{E_{\rm osc}} \tag{13}$$

Alternatively, the extended wavelength approximation of the single-term Sellmeier equation may be used to deal with the scattering parameters while maintaining the physical significance of the oscillator parameters. The formula expresses the relationship [29].

$$(n^2 - 1)^{-1} = \frac{1}{S_0 \lambda_0^2} - \frac{1}{\lambda^2 S_0}$$
 (14)

 $\lambda_0$  denotes the average oscillator parameter, and  $S_0$  represents the average oscillator strength.

A direct semi-empirical connection based on fundamental concepts is Miller's rule. It provides a way to use the linear refractive index, dispersion energy, and the energy of the effective oscillator in the Wemple-Di Domenico model to estimate the nonlinear refractive index  $(n_2)$  and nonlinear susceptibility  $(\chi^{(3)})$ . Below is a description of the relevant formula [31].

$$\chi^{(1)} = \frac{E_{\rm d}}{4\pi E_{\rm so}} \tag{15}$$

$$\chi^{(3)} = C\left[\left(\frac{n_o^2 - 1}{4\pi}\right)^4\right] \tag{16}$$

$$n_2 = \frac{12\pi\chi^{(3)}}{n_0} \tag{17}$$

In this framework,  $n_o$ , C,  $\chi^{(3)}$ , and  $\chi^{(1)}$  represent the refractive index, a constant value of  $1.7\times10^{-10}$ esu, nonlinear susceptibility, and linear susceptibility, respectively, they are uniform across all materials and irrespective of frequency.

By utilizing the material thicknesses as input, the linear attenuation coefficients ( $\mu$ ) can be determined through the equation provided below [32].

$$N=N_o e^{-\mu d}$$
 (18)

where  $\rm N_0$  represents an incident gamma ray, N signifies the attenuation of the gamma rays, and d denotes the thickness of the sample.

## **RESULTS AND DISCUSSION**

XRD analysis

Fig. 1 shows the XRD patterns of pure PVA and its nanocomposites. X-ray diffraction (XRD)

Table 1. The crystallite size obtained from XRD patterns using the Scherer formula for (SnO<sub>3</sub>-SiC) nanoparticles.

•			J	, , ,			
Material	Material 2Θ (°)		FWHM (rad)	Crystallite Size (nm)			
SnO <sub>2</sub>							
1	34	101	0.0082	18.255			
2	52	211	0.0083	19.221			
3	62	221	0.0113	14.883			
SiC							
1	38	101	0.0116	13.089			
2	55	211	0.0092	17.639			
3	66	221	0.0095	17.977			

was used to analyze the structure of PVA and the nanocomposites with varying concentrations of ( $SnO_2$ -SiC) nanoparticles to determine their structural composition. XRD study indicates

that both pure and doped ( $SnO_2$ -SiC) NCs have a broad band centered at  $2\theta$  =19.7°, according to XRD analysis, indicating the semi-crystalline nature of PVA. Intermolecular hydrogen bonding

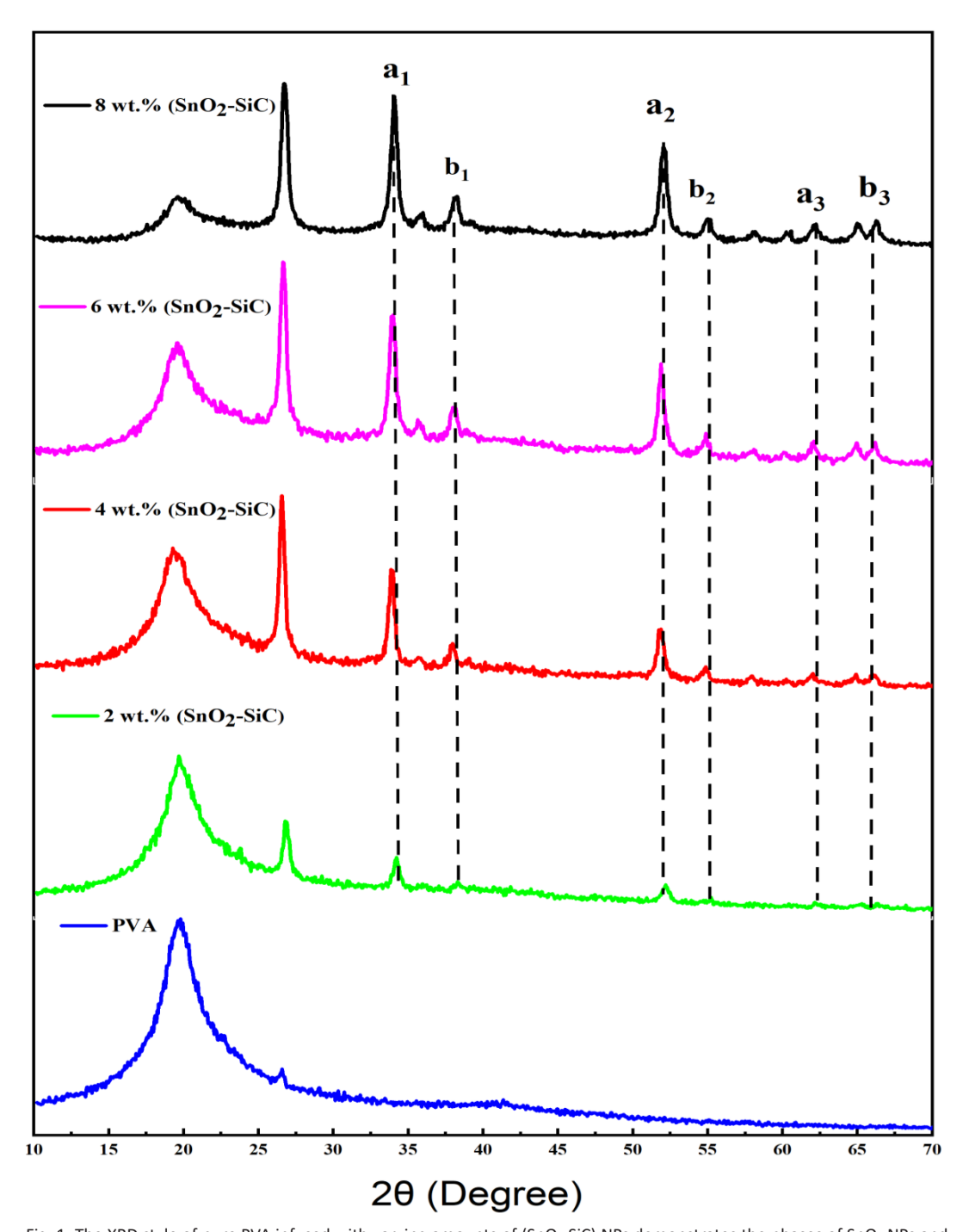


Fig. 1. The XRD style of pure PVA infused with varying amounts of  $(SnO_2-SiC)$  NPs demonstrates the phases of  $SnO_2$  NPs and SiC NPs, labeled as a and b, respectively.

serves as the principal mechanism that maintains the amorphous characteristics of PVA. This bond is formed by various monomer units and the molecules within each unit. The emergence of new peaks in the filled samples confirmed the presence of (SnO<sub>2</sub>-SiC) nanoparticle crystals within the polymeric samples. The results demonstrate that incorporating (SnO<sub>2</sub>-SiC) nanoparticles can change the structural features of the resulting films. The above result indicates that the SnO<sub>2</sub>-SiC nanoparticles were widely dispersed throughout the polymeric samples, which increased the

semi-crystalline ratio [33]. The improvement in conductivity is due to the changes in the crosslinking density, which leads to more defects in the nanocomposite samples, thus improving the ionic conductivity; this indicates that the incorporation of SnO<sub>2</sub>-SiC nanoparticles creates interactions between the SnO<sub>2</sub>-SiC nanoparticles and the polymeric matrix. The results indicate that incorporating SnO<sub>2</sub>-SiC nanoparticles can change the structural properties of the analyzed sample [34]. Table 1 shows the ranges, levels, and crystallite size of the SnO<sub>2</sub>-SiC nanoparticles.

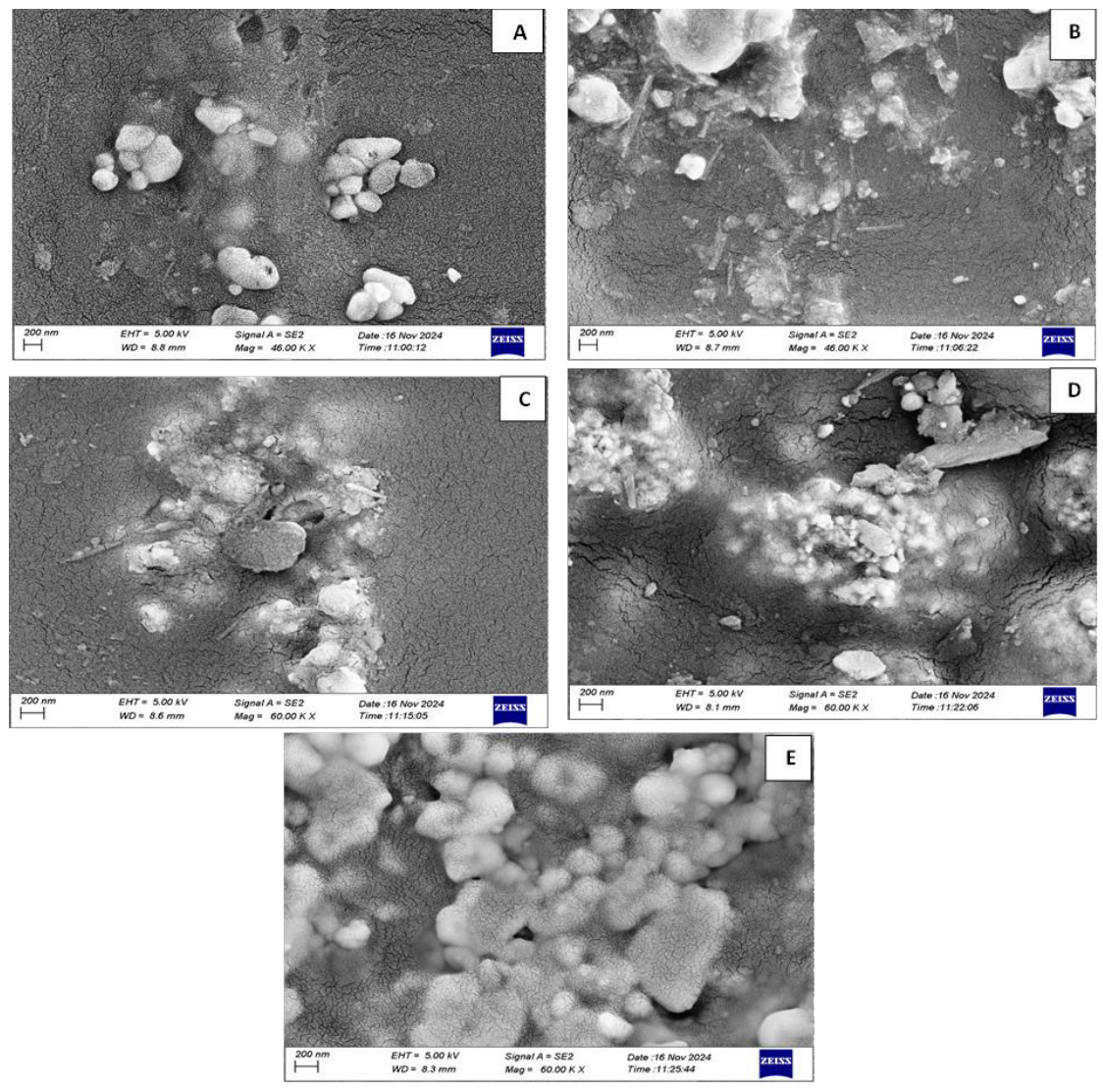


Fig. 2. SEM pictures of (PVA/SnO<sub>2</sub>-SiC) NCs: (A) for (PVA), (B) for 2 wt.% (SnO<sub>2</sub>-SiC), (C) for 4 wt.% (SnO<sub>2</sub>-SiC), (D) for 6 wt.% (SnO<sub>2</sub>-SiC), (E) for 8 wt.% (SnO<sub>3</sub>-SiC).

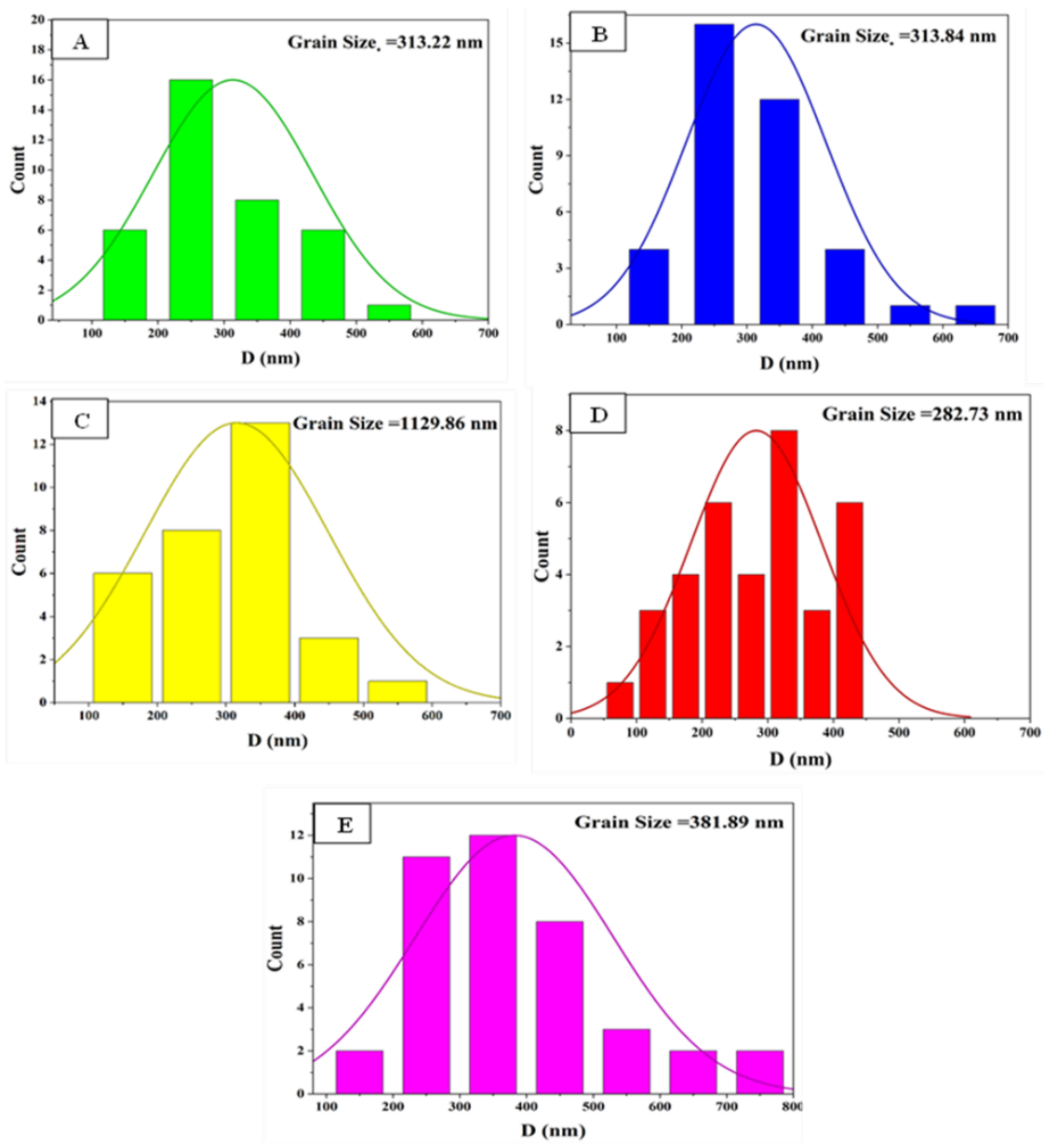


Fig. 3. Illustrates the grain size of (PVA/SnO $_2$ -SiC) NCs: (A) for (PVA), (B) for 2 wt% (SnO $_2$ -SiC), (C) for 4 wt% (SnO $_2$ -SiC), (D) for 6 wt% (SnO $_2$ -SiC), and (E) for 8 wt% (SnO $_2$ -SiC).

## Scanning Electron Microscope (SEM)

SEM is employed to comprehensively investigate the impact of tin dioxide and silicon carbide nanoparticle materials and analyze nanocomposite particles' dispersion in the polymer matrix. The typical SEM images of films formed from (PVA/SnO<sub>2</sub>-SiC) nanocomposites with and without varying the concentration of (SnO<sub>2</sub>-SiC) nanoparticles are depicted in Fig. 2.

The SEM images display white, differently sized rallies in Figures A, B, C, D, and E vary with the incremental increase in nanoparticle ratio; this may indicate a uniform growth process since several spherical particle clusters are scattered and sparsely distributed on the surface of the nanostructured films. The results indicate that the (SnO<sub>2</sub>-SiC) nanoparticles agglomerate and are uniformly distributed on films composed of (PVA/



SnO<sub>2</sub>-SiC) nanocomposites[35,36], as illustrated in images (B, C, D, and E). The particulate size of (PVA/SnO<sub>2</sub>-SiC) nanocomposites, as determined by SEM images, is illustrated in Fig. 3.

The components tin dioxide and silicon carbide (SnO<sub>2</sub>-SiC) are examined and identified using Energy Dispersive X-ray Spectroscopy (EDS), evident in Fig. 4A with the ratios of elements of C and O, 58.75 and 41.25, respectively, while Fig. 4B displays the EDX spectra of the elements of (PVA/SnO<sub>2</sub>-SiC) NCs and their ratios: C, O, Sn, and Si, 48.08, 27.05, 2.96, and 21.91, respectively. X-rays are high-energy photons generated via electronic shifts in the atoms of a solid object due to an incoming accelerated electron beam. The transitions are unique to each chemical

element. Primarily advanced Energy Dispersive X-ray Spectroscopy detection systems in electron microscopy, enhancing its application in the microstructural characterization of materials. Integrating EDS pictures and racial qualitative analysis using EDS has established it as one of the most potent instruments in scientific research [36].

The components tin dioxide and silicon carbide (SnO<sub>2</sub>-SiC) are examined and identified using Energy Dispersive X-ray Spectroscopy (EDS) clear in Fig. 4A with the proportions of components of (C) and (O), 58.75 and 41.25, respectively, while Fig. 4B displays the EDX spectra of the components of (PVA/SnO<sub>2</sub>-SiC) NCs and their proportions: C, O, Sn and Si, 48.08, 27.05, 2.96 and 21.91, respectively.

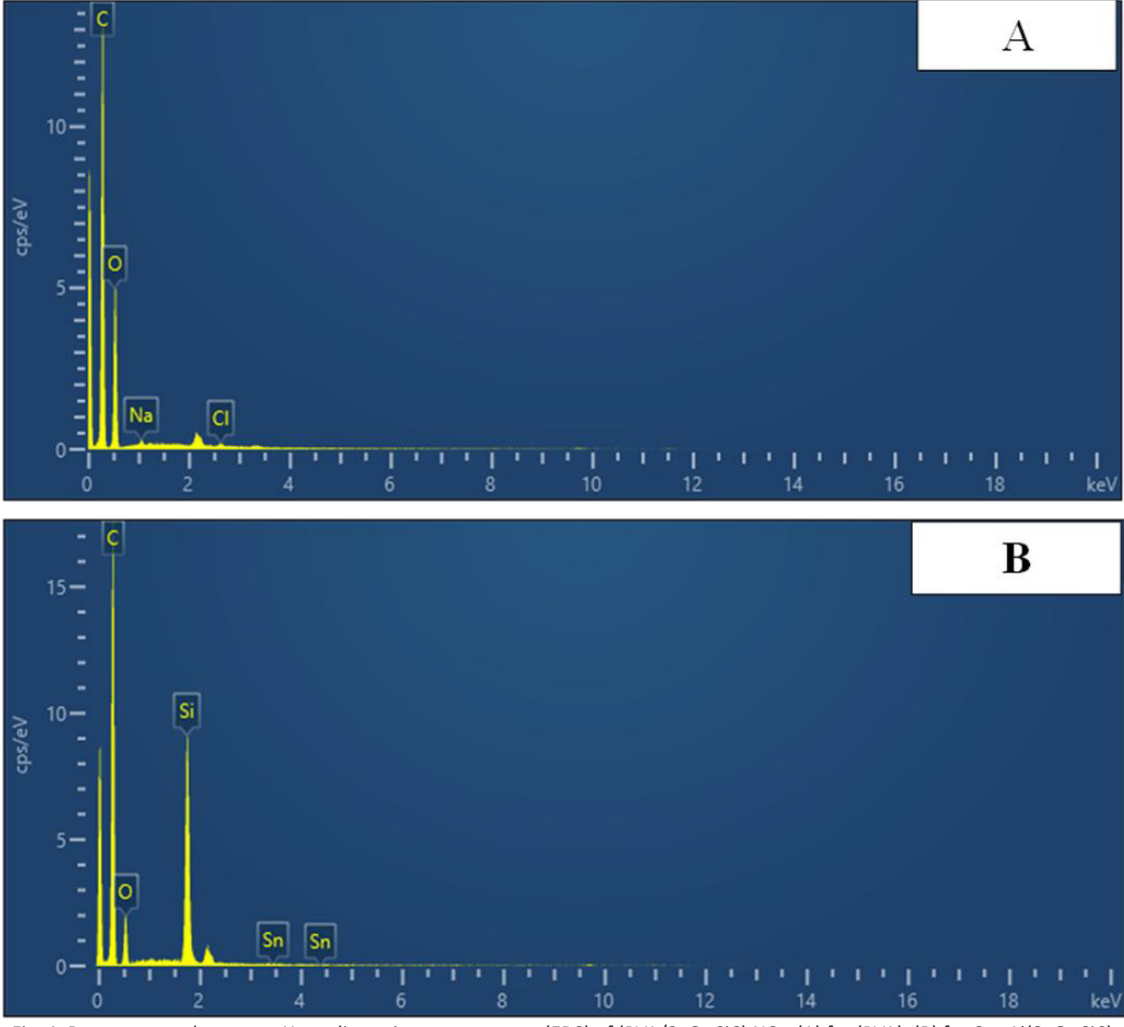


Fig. 4. Demonstrate the energy X-ray dispersion spectroscopy (EDS) of (PVA/SnO<sub>2</sub>-SiC) NCs: (A) for (PVA), (B) for 6 wt%(SnO<sub>2</sub>-SiC).

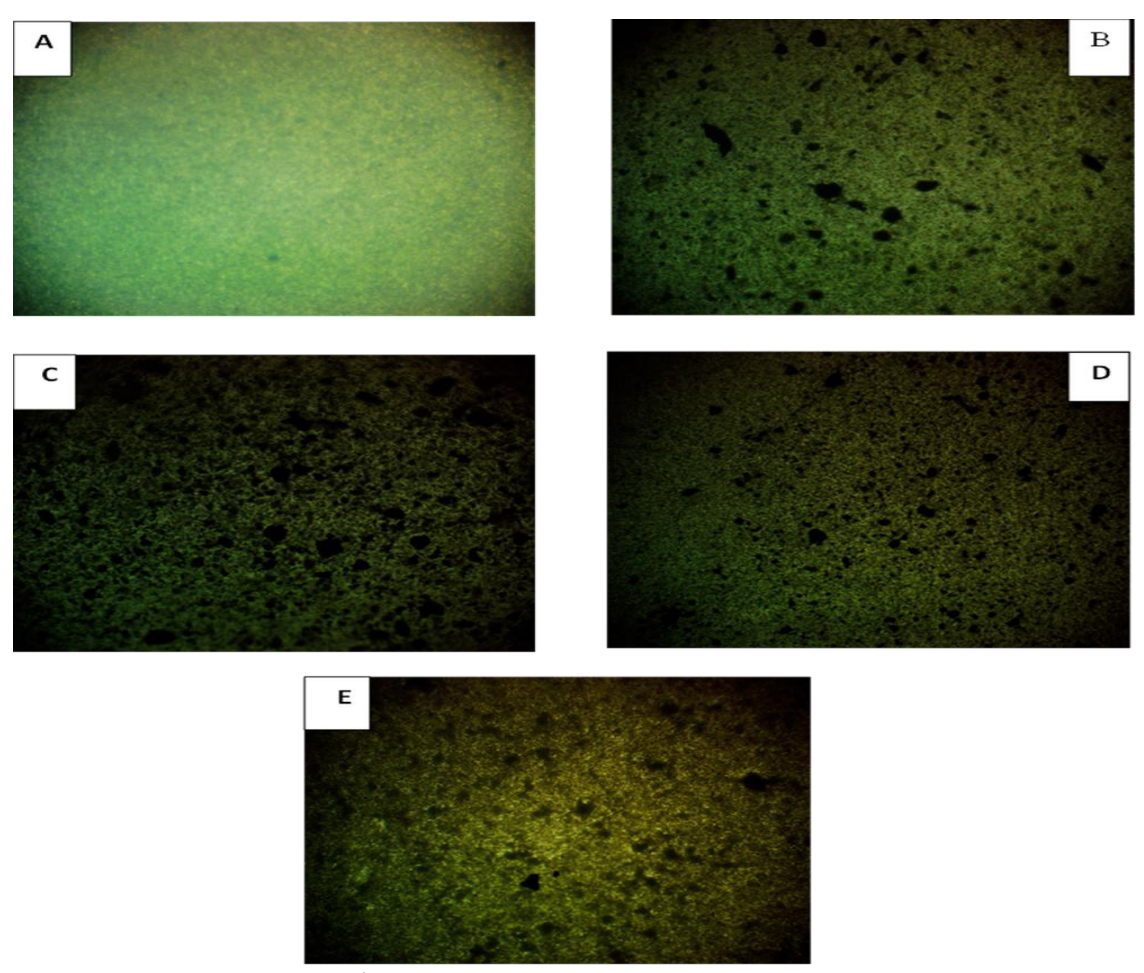


Fig. 5. Photomicrographs (10X) for (PVA/SnO $_2$ -SiC) nanocomposites: (A) (PVA), (B) 2 wt% SnO $_2$ -SiC, (C) 4 wt% SnO $_2$ -SiC, (D) 6 wt% SnO $_2$ -SiC, (E) 8 wt% SnO $_2$ -SiC.

X-rays are high-energy photons generated via electronic shifts in the atoms of a solid object due to an incoming accelerated electron beam. The transitions are unique to each chemical element. Predominantly facilitated the advancement of Energy Dispersive X-ray Spectroscopy detection systems in electron microscopy, expanding its use in materials' microstructural characterization. Additionally, the combination of EDS imaging and elemental qualitative analysis provided via EDS rendered it one of the most potent instruments in scientific research [37].

# Optical Microscope of PVA/SnO<sub>3</sub>-SiC NCs

Fig. 5 presents optical microscope images (OM) photos of the pure PVA and the PVA integrated with (SnO<sub>2</sub>-SiC) Nanoparticles films at

varying focus. The photos were captured using a magnification strength of 10X. The images illustrate significant discrepancies in the midst of them (A, B, C, D, and E). A network forms throughout the significant phase of the (PVA) pure. When (SnO<sub>3</sub>-SiC) nanoparticles increase, more connective pathways form. The microscopic images provide evident visual evidence of discernible distinctions among the samples as the quantities of (SnO<sub>2</sub>-SiC) nanoparticles are progressively increased. The tiny SnO<sub>2</sub>-SiC nanoparticles create a continuous structure within the polymer matrix in PVA membranes at 8% by weight. The presence of specific channels in the network facilitates the movement of charge carriers, leading to a decrease in the resistivity of the pure polyvinyl alcohol (PVA) material [38].



## FTIR Analysis of PVA/SnO<sub>2</sub>-SiC PNCs

An infrared spectrometer (FTIR) is employed to ascertain the types of bonds formed between the materials, specifically to identify the nature of the bonds constituting the resultant mixture, thereby differentiating between a chemical reaction and a physical reaction involving the PVA polymer and SnO<sub>2</sub>-SiC nanoparticles. Fig. 6 shows the infrared spectrum of the nanocomposite (PVA/SnO<sub>2</sub>-SiC), as each group of infrared spectra is characteristic of certain bonds of the material within a wavenumber range ranging from (800 - 4000) cm<sup>-1</sup>. All of PVA's main bonds are present in the (PVA/SnO<sub>2</sub>-SiC) nanocomposite films, according to the FTIR analysis. But because of the addition

of (SnO<sub>2</sub>-SiC) NMs, which affect the infrared absorption, the absorption intensity differs from that of pure PVA. The absorption peaks therefore diverge from their initial levels[39]. The functional groups of polyvinyl alcohol (PVA) were observed at wavenumbers 3284.7, 2938.2, 1733.2, and 1087.3 cm<sup>-1</sup>, which corresponded to the stretching vibrations of hydroxyl groups (O–H), which may be attributed to the stretching vibrations of C-H bonds, the stretching mode of the C=C bond, and bending vibrations of C-O, respectively. The bands observed at a wavenumber of 837.8 cm<sup>-1</sup> are attributed to the bending vibrations of the C=O bonds [40]. The infrared spectral behavior of polymeric films post-addition of (SnO<sub>2</sub>-SiC) aligns

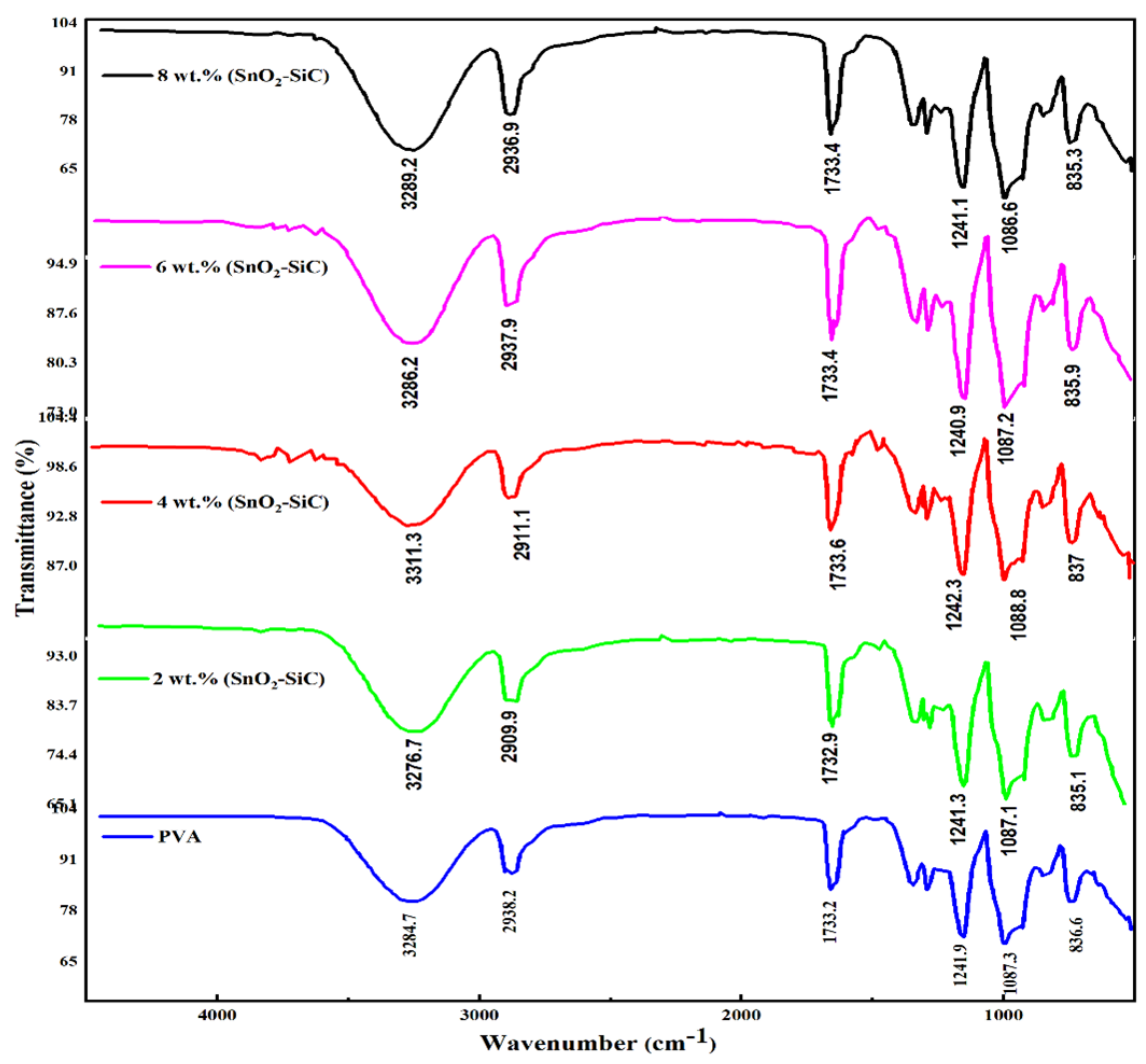
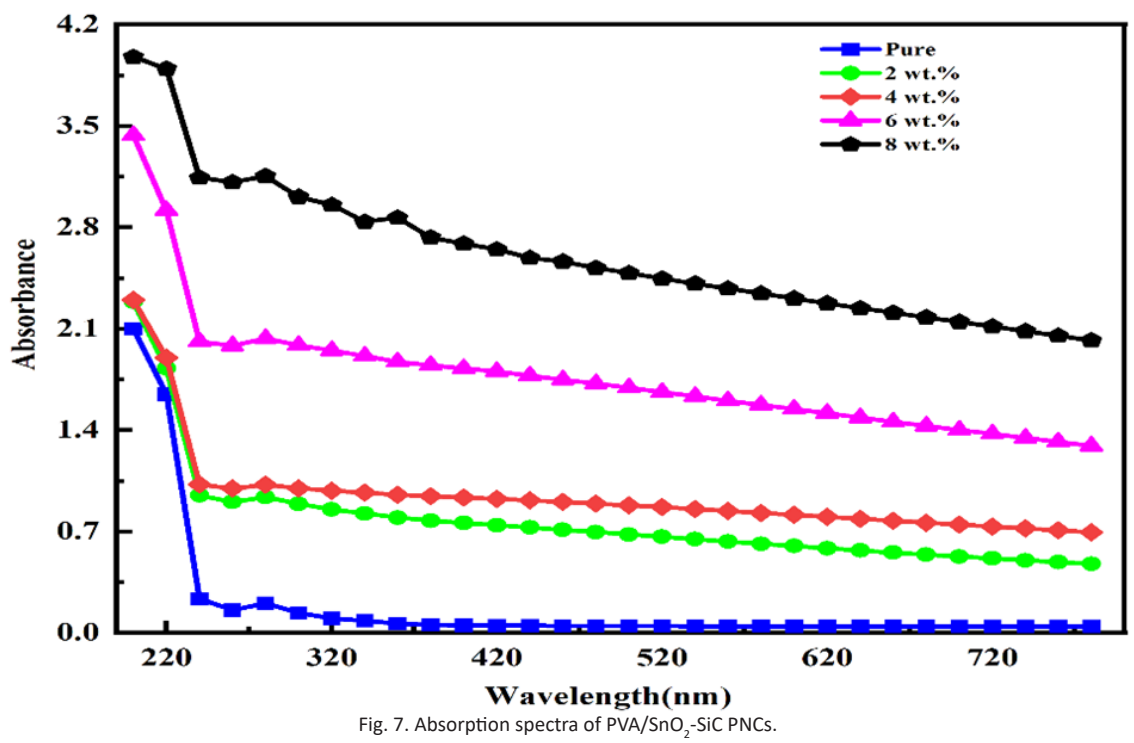
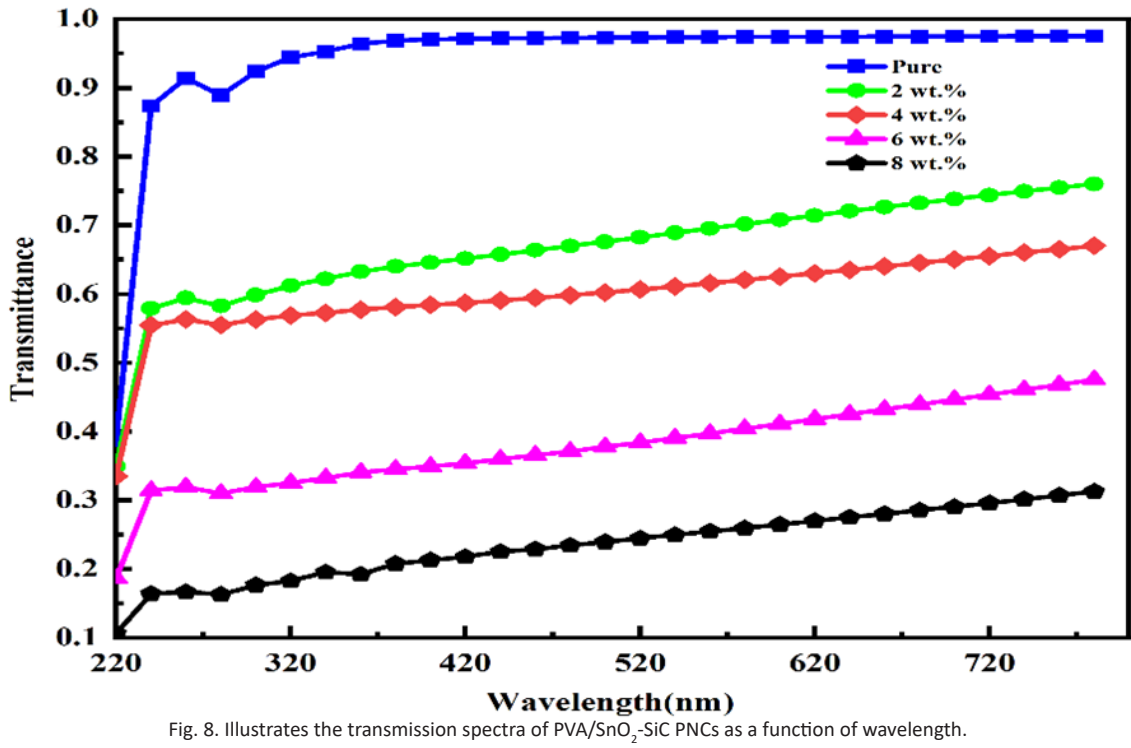


Fig. 6. PVA/SnO<sub>2</sub>-SiC PNCs FTIR spectra.





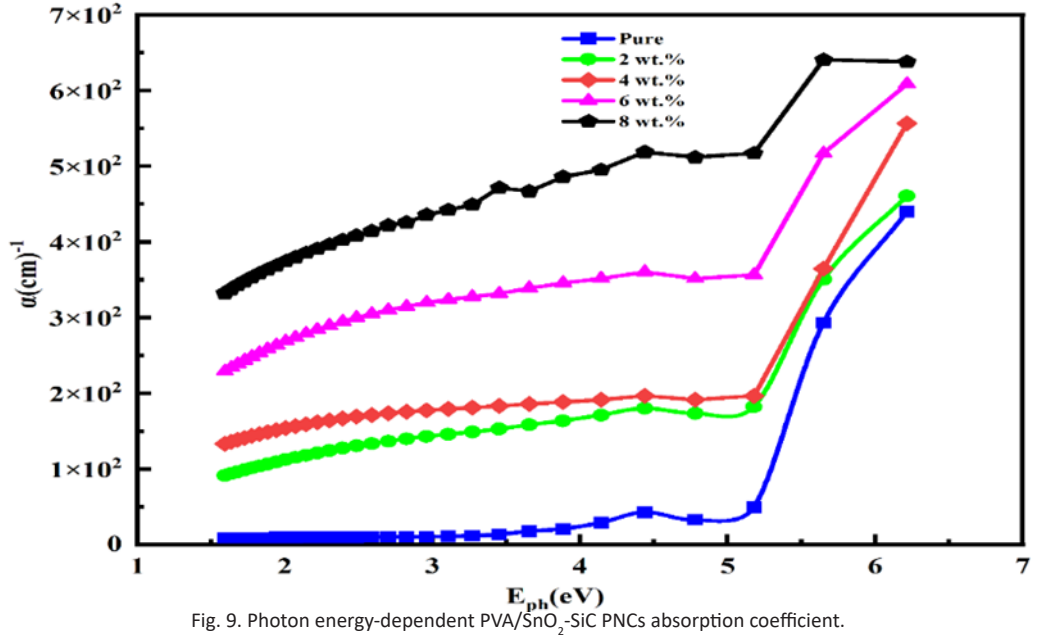
with that of the polymeric membrane prior to the addition, with minor alterations attributed to bond vibrations; this suggests the absence of a chemical reaction between the nanocomposite materials, indicating a physical interaction instead.

The nonlinear and linear optical properties of PVA/ SnO<sub>3</sub>-SiC Nanocomposites

The optical absorbance and transmittance spectra of the PVA mix including SnO<sub>2</sub>-SiC are depicted in Figs. 7 and 8, spanning a wavelength ambit from (200 to 780 nm). Fig. 7 illustrates that all nanocomposite specimens exhibited significant absorption in the ultraviolet band. This phenomenon may be elucidated by the elevated energy of photons, enabling them to engage with atoms and elevate electrons of inferior to higher energy states. The absorption of nanocomposite specimens in the visible spectra and close to-infrared is negligible, because to the insufficient energy of the input photons to interact in conjunction to the atoms. The intensity of film absorption is higher at lesser wavelengths and decreases as the wavelength lengthens. The augmentation of SnO<sub>3</sub>-SiC particle concentration results in a corresponding rise in absorption, hence amplifying the quantity of charge carriers. The noticed phenomenon can be elucidated by the quantity of energy levels established by

impurity atoms located inside the valence and conduction bands. These levels allow electrons to migrate, which in turn absorbs photons with energies inferior to the incoming photons' optical energy gap[41]. Fig. 8 illustrates the transmittance of undoped PVA and PVA doped with SnO<sub>3</sub>-SiC. The decrease in transmittance is associated with the increasing mass of SnO<sub>2</sub>-SiC. This behavior is anticipated due to the incorporation and dispersion of nanoparticles inside the polymer sheets, resulting in the scattering of incident photons [42].

Fig. 9 illustrates the absorption coefficient ( $\alpha$ ) according to the energy of the incident photons. The graph indicates that the absorption coefficient of each nanocomposite material specimen diminishes with decreasing energies, implying that the energy is insufficient for the electron to transition than its Equivalence range to the conduction range. In contrast, at elevated energy levels, absorption markedly intensifies, signifying a substantial probability of the electron transitioning from the Equivalence range to the conduction range. The fallen photon's energy exceeds the forbidden energy gap, leading to conduction. The absorption coefficient of nanocomposites rises with increased nanoparticle concentrations, since topical energy levels emerge inside the conduction band, enhancing the absorption of



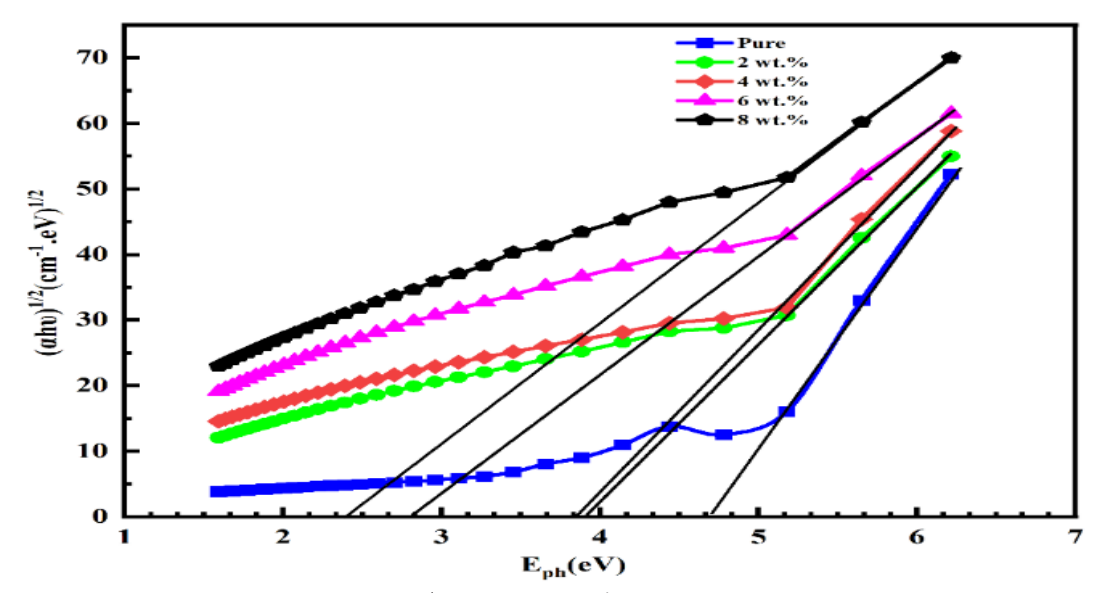


Fig. 10.  $(\alpha h u)^{1/2}$  difference for PVA/SnO<sub>2</sub>-SiC PNCs with E<sub>nh</sub>

incident photons [43]. The absorbance coefficient for (PVA/SnO<sub>2</sub>-SiC) PNCs is determined to be under 104 cm<sup>-1</sup>, indicating the existence in an indirect energy band gap.

The effect of the stuffing weight ratio (SnO<sub>2</sub>-SiC) on the bandgap width (E<sub>a</sub>) of (PVA/SnO<sub>2</sub>-SiC) PNCs is examined in this study. The energy difference between the lowest vacant molecular orbitals and the highest occupied molecular orbitals is known as the optical band gap (E<sub>g</sub>). Figs. 10 and 11 depict the absorbance edge graphs, represented as  $(\alpha h u)^{1/2}$  and  $(\alpha h u)^{1/3}$ , with the photon energy of the films in relation to the fallen photon energy (hv) for both permitted and prohibited transitions. The permitted band gap energy (AE<sub>2</sub>) was ascertained by extending the linear segments of the shown curves to the juncture where the incoming photon energy approaches zero. The energy difference related to the permitted indirect transition may be approximated by drawing a straight line from the apex of the curve to the x-axis at the point where the square root of  $(\alpha h \upsilon)$ equals zero. Table 2 displays the relevant values, affirming the consistency of the measured AE values for each film. The bandgap energy of pure PVA is around 4.71 eV. The addition of 8 wt% SnO<sub>3</sub>-SiC to PVA results in the creation of (PVA/SnO<sub>2</sub>-SiC) nanocomposites, which have a reduced E value of 2.40 eV relative to pure PVA. This decrease is ascribed to the formation of secondary energy levels inside the bandgap of pure PVA. Moreover, the incorporation of  ${\rm SnO}_2$ -SiC into PVA leads to a significant reduction in the forbidden bandgap energy (FE  $_{\rm g}$ ) values, as seen in Fig. 11. The fluctuation in FE  $_{\rm g}$ , from 4.23 eV to 0.72 eV, is mostly ascribed to the emergence of energy levels inside the bandgap of the host material. The addition of fillers leads to an augment in voids, structural disorder, and flaws within the composite matrix, which, therefore, reduces FE  $_{\rm g}$  values [44] .

Furthermore, the optical transition between the localized and band states is documented using Urbach's tail values. The h $\nu$  versus slope of the straight lines of ln ( $\alpha$ ) can be used to calculate the band tail of the PVA/SnO $_2$ -SiC films, as illustrated in Fig. 12. Table 2 lists the band tail values of the films under examination. The band tail value of the PVA is 0.26 eV, as is evident. For 2%, 4%, 6%, and 8% films, the value increases to 0.71, 0.76, 1.26 and 2.19 eV, respectively. These results corroborate the significant induced SnO $_2$ -SiC Nanoparticles on the energy states following insertion and demonstrate the presence of additional defect states within the PVA [45].

By plotting  $(hv)^2$  versus  $(n^2-1)^{-1}$  yields a linear graph, with a slope of  $1/E_d$   $E_{osc}$  and where the intercept corresponds to  $E_{osc}$   $E_d$ , as seen in Fig. 13. The measured values of  $E_0$  diminished with rising nanoparticle concentration, presumably due to an increase in scattering centers and a consequent

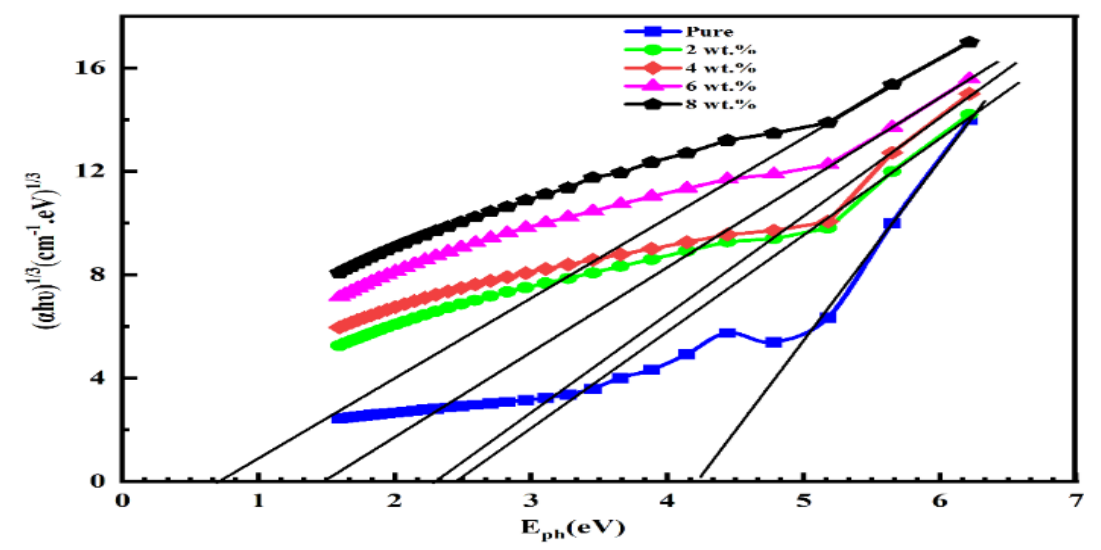


Fig. 11.  $(\alpha h u)^{1/3}$  difference of PVA/SnO<sub>2</sub>-SiC PNCs with E<sub>nh</sub>

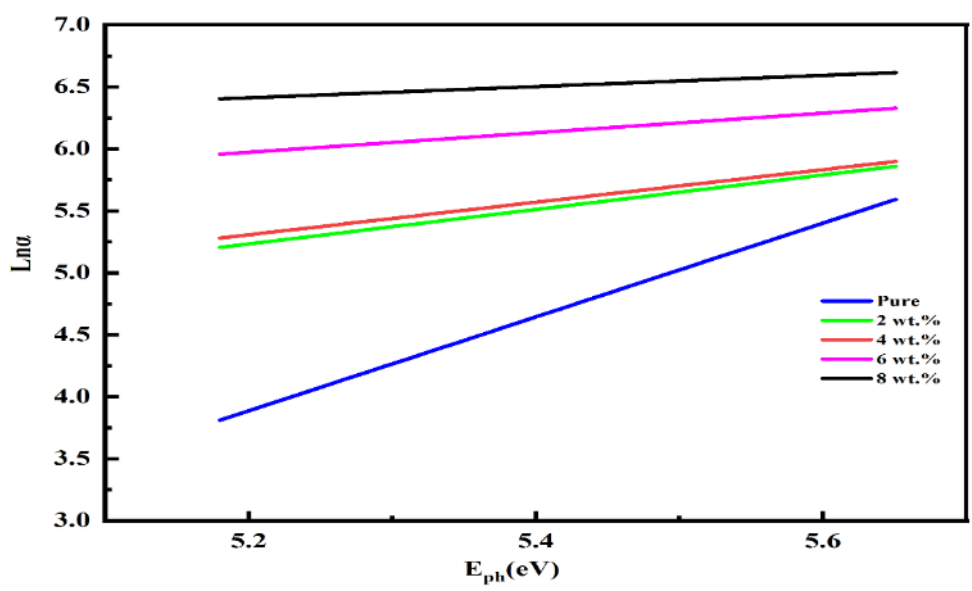


Fig. 12. Illustrates the plot of ln  $\alpha$  versus hv for the purpose of determining Urbach energy.

drop in band gap energy. The reduction in  $\rm E_{\rm osc}$  and  $\rm E_{\rm d}$  with increased nanomaterial concentration indicates changes in the scattering and refractive properties of light. In photovoltaic applications, these attributes are essential for comprehending the interaction of light with a material. The Ed relates to the impact of electrical fields from outside on the material, possibly improving

the pictures' conversion efficiency. A decrease in  $\rm E_{\rm osc}$  signifies that the material demonstrates heightened allergy to low energy, therefore enhancing absorption across a wider spectrum.

The zero-frequency refractive index  $(n_0)$  and dielectric constant  $(\epsilon_0)$  display a gradual augment with the rise in nanoparticle weight  $(n_0)$  increases from 1.25 to 3.60,  $\epsilon_0$  from 1.57 to 12.98);

this can be understood as an outcome of the nanocomposites gaining enhanced polarizability due to the incorporation of  $SnO_2$ -SiC. With the increase in filler content, the material exhibits greater optical density, resulting in an elevated refractive index [46]; These data are also included in Table 2.

A linear connection with a slope of  $1/S_0$  and an intercept of  $1/S_0\lambda_0^2$  may be obtained by plotting  $\lambda^{-2}$  versus  $(n^2-1)^{-1}$ , as shown in Fig. 14.  $\lambda_0$  grows with increasing nanoparticle concentration. This shift to longer wavelengths indicates increased sensitivity to lower-energy (longer-wavelength) photons close to the visible and infrared spectrum.

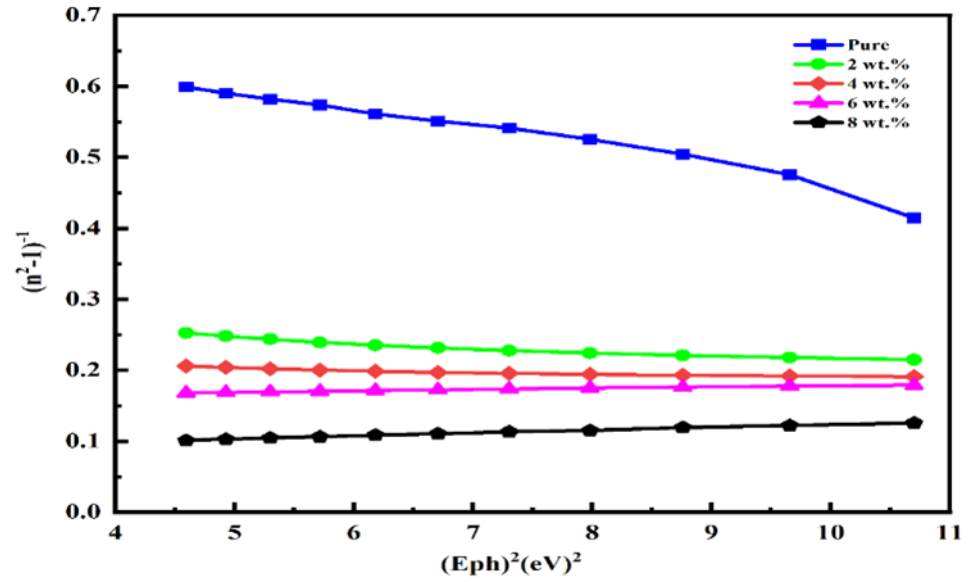


Fig. 13. Illustrates the plot to determine the single oscillator energy ( $E_{osc}$ ) and the dispersion energy ( $E_{d}$ ).

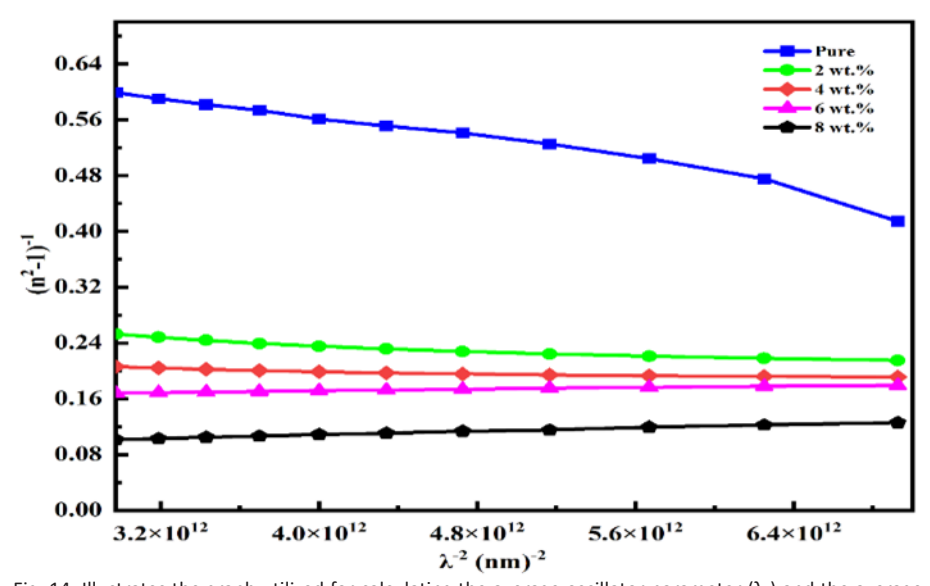


Fig. 14. Illustrates the graph utilized for calculating the average oscillator parameter ( $\lambda_0$ ) and the average oscillator strength ( $S_0$ ).

Table 2. Optical parameters for PVA/SnO<sub>2</sub>-SiC PNCs.

NPs wt.%	AE <sub>g</sub> (eV)	FE <sub>g</sub> (eV)	E <sub>u</sub> (eV)	E <sub>d</sub> (eV)	E <sub>osc</sub> (eV)	S <sub>o</sub> (m <sup>-2</sup> )	λ <sub>0</sub> (m)	n <sub>o</sub>	εο	X <sup>(1)</sup>	X <sup>(3)</sup> (esu)	n₂ (esu)
0	4.71	4.23	0.26	58.14	9.46	<sup>14</sup> 3.49×10	- <sup>7</sup> 1.31×10	1.25	1.57	0.04	7.62×10 <sup>-16</sup>	2.28×10 <sup>-14</sup>
2	3.91	2.46	0.71	54.50	9.29	2.69×10 <sup>14</sup>	-71.33×10	2.15	4.63	0.28	1.19×10 <sup>-12</sup>	2.08×10 <sup>-11</sup>
4	3.86	2.30	0.76	44.07	7.97	1.60×10 <sup>14</sup>	⁻ <sup>7</sup> 1.55×10	2.37	5.657	0.37	3.21×10 <sup>-12</sup>	5.09×10 <sup>-11</sup>
6	2.82	1.51	1.26	24.52	6.75	<sup>14</sup> 1.07×10	<sup>-7</sup> 1.84×10	2.69	7.25	0.49	1.04×10 <sup>-11</sup>	1.46×10 <sup>-10</sup>
8	2.40	0.72	2.19	4.61	4.54	<sup>13</sup> 2.38×10	<sup>-7</sup> 2.73×10	3.60	12.98	0.95	1.41×10 <sup>-10</sup>	1.47×10 <sup>-9</sup>

The material's ability to absorb light at lower energy levels is shown by the change in  $\lambda_0$ , which is advantageous for infrared and photovoltaic applications. The capacity of the material to absorb light in this range further enhances its adaptability for optoelectronic devices, particularly those that are intended to leverage a broader spectrum of solar energy.  $S_0$  levels tend to decrease. A substance with a low  $S_0$  value has a higher capacity to absorb light, which means it interacts with incoming light more effectively and facilitates greater photon absorption [30].

Nonlinear optics, optical switching, and frequency conversion are areas where this material excels since both the nonlinear susceptibility  $(\chi^{(3)})$  and linear susceptibility  $(\chi^{(1)})$  have a similar trend of increasing values as the concentration of nanoparticles increases. The nonlinear optical response seems to have been enhanced.

As nanoparticle loading increases, the nonlinear refractive index  $(n_2)$  increases from  $2.28\times10^{-14}$  esu to  $1.47\times10^{-9}$  esu. This improvement enhances the material's potential for nonlinear optical applications[31]; Table 2 also includes these values.

## CONCLUSION

This work aimed to fabricate (PVA/SnO<sub>2</sub>-SiC) PNCs and analyze their structural, optical nonlinear and linear and morphological characteristics. The FTIR spectra indicate a physical interaction between the pure polymer and the (SnO<sub>2</sub>-SiC) nanoparticles. XRD shows that the crystalline rate of nanocomposites increase by increasing of (SnO<sub>2</sub>-SiC) nanoparticles. The FE-SEM examination findings show that the surface morphology is uniformly distributed and outstanding. As the wavelength increases, the transmittance

characteristic of the (PVA/SnO<sub>2</sub>-SiC) PNCs shows that they become more transparent, which is consistent with a decrease in absorption. However, the composite shows decreased transmittance and increasing absorbance when the concentration is raised. The nonlinear refractive index (n<sub>3</sub>), linear susceptibility ( $\chi^{(1)}$ ), Urbach tail energy E<sub>..</sub>, zero frequency dielectric constant  $\varepsilon_{o}$ , nonlinear susceptibility ( $\chi^{(3)}$ ), zero frequency refractive index  $n_0$ , and average oscillator parameter  $\lambda_0$  demonstrate an increase with the addition of nanoparticles. On the contrary, there is a decline observed in the dispersion energy E<sub>d</sub>, single-oscillator energy E<sub>oso</sub>, and average oscillator strength S<sub>0</sub>. The integration of a nanofiller consisting of 8 wt.% of (SnO<sub>3</sub>-SiC) led to a reduction in the energy gap for both indirect transitions, regardless of their permissibility. The allowed energy gap decreased from 4.71 to 2.40 eV, while the forbidden energy gap decreased from 4.23 to 0.72 eV. This results confirms the potential use of these materials in different optical applications. The (PVA/SnO<sub>3</sub>-SiC) nanocomposites have highest attenuation coefficients for gamma radiation. These results indicate that the (PVA/ SnO<sub>3</sub>-SiC) nanocomposites promising materials for use in optoelectronic nanodevices and gamma radiation shielding.

## **CONFLICT OF INTEREST**

The authors declare that there is no conflict of interests regarding the publication of this manuscript.

## **REFERENCES**

- Abdulridha IK, Naser BA. Optical Properties of Malachite Green Organic Laser Dye Doped with PMMA Polymer and Cu Nanoparticles. Neuroquantology. 2022;20(3):259-264.
- Bezza FA, Tichapondwa SM, Chirwa EMN. Fabrication of monodispersed copper oxide nanoparticles with potential

- application as antimicrobial agents. Sci Rep. 2020;10(1).
- 3. Hu H, Onyebueke L, Abatan A. Characterizing and Modeling Mechanical Properties of Nanocomposites-Review and Evaluation. Journal of Minerals and Materials Characterization and Engineering. 2010;09(04):275-319.
- Basavaraja C, Kim BS, Huh DS. Characterization and AC electrical conductivity for the dispersed composites containing alginate-multiwalled carbon nanotubes. Macromolecular Research. 2011;19(3):233-242.
- Awwad NS, Ibrahium HA, Abd El-Kader MFH, Elhosiny Ali H, Mostafa AM, Menazea AA. Improvement in electrical conductivity characterization of chitosan/Poly (ethylene oxide) incorporated with V<sub>2</sub>O<sub>5</sub> NPs via laser ablation. Journal of Materials Research and Technology. 2022;16:1272-1282-
- Ahmed MK, Moydeen AM, Ismail AM, El-Naggar ME, Menazea AA, El-Newehy MH. Wound dressing properties of functionalized environmentally biopolymer loaded with selenium nanoparticles. J Mol Struct. 2021;1225:129138.
- Soliman TS. Effects of SiO2 Nanoparticles on Polyvinyl Alcohol/Carboxymethyl Cellulose Polymer Blend Films' Structural, Wettability, Surface Roughness, and Optical Characteristics. Adv Polym Tech. 2024;2024:1-10.
- Pendhari SS, Kant T, Desai YM. Application of polymer composites in civil construction: A general review. Compos Struct. 2008;84(2):114-124.
- El Fewaty NH, El Sayed AM, Hafez RS. Synthesis, structural and optical properties of tin oxide nanoparticles and its CMC/PEG-PVA nanocomposite films. Polymer Science Series A. 2016;58(6):1004-1016.
- 10. Habeeb MA, Al-Sharifi NK. Improvement structural and dielectric properties of PS/SiC/Sb<sub>2</sub>O<sub>3</sub> nanostructures for nanoelectronics devices. East European Journal of Physics. 2023(2):341-347.
- Costa-Marrero Y, Andrade M, Ellena J, Duque-Rodríguez J, Farias T, Autié-Castro G. Zeolite/ZnO composites based on a Cuban natural clinoptilolite and preliminary evaluation in methylene blue adsorption. Materials Research Express. 2020.
- Crosby AJ, Lee JY. Polymer Nanocomposites: The "Nano" Effect on Mechanical Properties. Polymer Reviews. 2007;47(2):217-229.
- Bhavsar S, Patel GB, Singh NL. Investigation of optical properties of aluminium oxide doped polystyrene polymer nanocomposite films. Physica B: Condensed Matter. 2018;533:12-16.
- 14. Dutra DAM, Pereira GKR, Kantorski KZ, Valandro LF, Zanatta FB. Does Finishing and Polishing of Restorative Materials Affect Bacterial Adhesion and Biofilm Formation? A Systematic Review. Oper Dent. 2018;43(1):E37-E52.
- Jaber ZS, Habeeb MA, Radi WH. Synthesis and Characterization of (PVA-CoO-ZrO<sub>2</sub>) Nanostructures for Nanooptoelectronic Fields. East European Journal of Physics. 2023(2):228-233.
- Marikkannan M, Vishnukanthan V, Vijayshankar A, Mayandi J, Pearce JM. A novel synthesis of tin oxide thin films by the sol-gel process for optoelectronic applications. AIP Advances. 2015;5(2).
- 17. Habeeb MA, Mahdi SM. Influence of ZrC nanofiler on the structural, dielectric and optical features of the PVA–PVP blend for electronic and optical nanodevices. Optical and Quantum Electronics. 2023;55(12).
- 18. Soliman TS, Vshivkov SA. Effect of Fe nanoparticles on the structure and optical properties of polyvinyl alcohol

- nanocomposite films. Journal of Non-Crystalline Solids. 2019:519:119452.
- Gautam A, Ram S. Preparation and thermomechanical properties of Ag-PVA nanocomposite films. Materials Chemistry and Physics. 2010;119(1-2):266-271.
- Srikanth C, Sridhar BC, Prasad MVNA, Mathad RD. Characterization and DC Conductivity of Novel ZnO Doped Polyvinyl Alcohol (PVA) Nano-Composite Films. Journal of Advanced Physics. 2016;5(2):105-109.
- 21. Mondal S. Polymer Nano-Composite Membranes. Journal of Membrane Science and Technology. 2015;05(01).
- Allen PB. Elementary Solid State Physics: Principles and Applications by M. A. Omar. Am J Phys. 1975;43(10):929-933.
- 23. Mohammed AA, Habeeb MA. Effect of Si<sub>3</sub>N<sub>4</sub>/ TaC nanomaterials on the structural and electrical characteristics of poly methyl methacrylate for electrical and electronics applications. East European Journal of Physics. 2023(2):157-164.
- 24. Soliman TS, Vshivkov SA, Hessien MM, Elkalashy SI. Impact of Mn–Ni spinal ferrite nanoparticles on the structural, morphological, surface roughness, and optical parameters of polyvinyl alcohol for optoelectronic applications. Soft Matter. 2023;19(40):7753-7763.
- 25- Baker MI, Walsh SP, Schwartz Z, Boyan BD. A review of polyvinyl alcohol and its uses in cartilage and orthopedic applications. Journal of Biomedical Materials Research Part B: Applied Biomaterials. 2012;100B(5):1451-1457.
- Heiba ZK, Mohamed MB, Badawi A, Alhazime AA. The role of Cd0.9Mg0.1S nanofillers on the structural, optical, and dielectric properties of PVA/CMC polymeric blend. Chem Phys Lett. 2021;770:138460.
- 27. Algidsawi AJK, Hashim A, Hadi A, Habeeb MA. Exploring the characteristics of SnO<sub>2</sub> nanoparticles doped organic blend for low cost nanoelectronics applications. Semiconductor Physics, Quantum Electronics and Optoelectronics. 2021;24(04):472-477.
- 28. Abdelaziz M, Abdelrazek EM. Effect of dopant mixture on structural, optical and electron spin resonance properties of polyvinyl alcohol. Physica B: Condensed Matter. 2007;390(1-2):1-9.
- 29. Fasasi AY, Ajenifuja E, Osagie E, Animashaun L, Adeoye A, Obiajunwa E. Optical, Dielectric and Optoelectronic Properties of Spray Deposited Cu-doped Fe2O3 Thin Films. Journal of the Nigerian Society of Physical Sciences. 2023:1180.
- 30- Al-Zahrani JH, El-Hagary M, El-Taher A. Gamma irradiation induced effects on optical properties and single oscillator parameters of Fe-doped CdS diluted magnetic semiconductors thin films. Mater Sci Semicond Process. 2015;39:74-78.
- 31. El-naggar AM, Alsulaymani LA, Bakr Mohamed M, Alsaleh AA, Kamal AM, Albassam AA, et al. Influence of nature melanin on the structural, linear/nonlinear optical properties and electrical conduction mechanism of PVA/ CMC/PPy blended polymers for optoelectronic applications. Results in Physics. 2024;64:107924.
- 32. Oreibi I, Ali Habeeb M, Abdul Hamza RS. Polymer nanocomposites comprising PVA matrix and Ag-BaTiO<sub>3</sub> nanofillers: a comparative study of structural, dielectric and optical characteristics for optics and quantum nanoelectronic applications. Optical and Quantum Electronics. 2023;56(1).



- Abdullah OG, Aziz SB, Rasheed MA. Structural and optical characterization of PVA:KMnO4 based solid polymer electrolyte. Results in Physics. 2016;6:1103-1108-
- 34. Abdulwahid RT, Abdullah OG, Aziz SB, Hussein SA, Muhammad FF, Yahya MY. The study of structural and optical properties of PVA:PbO<sub>2</sub> based solid polymer nanocomposites. Journal of Materials Science: Materials in Electronics. 2016;27(11):12112-12118.
- 35. Habeeb MA, Hamza RSA, Oreibi I, Sabur DA. Fabrication and Evaluation the Optical and Dielectric Characteristics of Promising PVA-ZrC-SiO<sub>2</sub> Nanocompsites Films. Silicon. 2024;16(7):2839-2851.
- 36. Bell DC, Garratt-Reed AJ. Energy Dispersive X-ray Analysis in the Electron Microscope: Garland Science; 2003 2003/07/10.
- Determination of Optical Parameters of Polymer Blend/ Nanoceramics for Electronics Applications. Nanosistemi, Nanomateriali, Nanotehnologii. 2021;19(2).
- 38. Ravi M, Pavani Y, Kiran Kumar K, Bhavani S, Sharma AK, Narasimha Rao VVR. Studies on electrical and dielectric properties of PVP:KBrO4 complexed polymer electrolyte films. Materials Chemistry and Physics. 2011;130(1-2):442-448.
- 39. Liu P, Chen W, Liu C, Tian M, Liu P. A novel poly (vinyl alcohol)/ poly (ethylene glycol) scaffold for tissue engineering with a unique bimodal open-celled structure fabricated using supercritical fluid foaming. Sci Rep. 2019;9(1).
- 40. Ikhmayies SJ, Ahmad-Bitar RN. An investigation of the

- bandgap and Urbach tail of vacuum-evaporated  ${\rm SnO_2}$  thin films. Renewable Energy. 2013;49:143-146.
- Alrowaili ZA, Taha TA, El-Nasser KS, Donya H. Significant Enhanced Optical Parameters of PVA-Y2O3 Polymer Nanocomposite Films. Journal of Inorganic and Organometallic Polymers and Materials. 2021;31(7):3101-3110
- 42. Alshammari AH. Structural, Optical, and Thermal Properties of PVA/SrTiO<sub>3</sub>/CNT Polymer Nanocomposites. Polymers. 2024;16(10):1392.
- Srivastava S, Haridas M, Basu JK. Optical properties of polymer nanocomposites. Bull Mater Sci. 2008;31(3):213-217.
- 44. Algidsawi AJK, Hashim A, Hadi A, Habeeb MA, Abed HH. Influence of MnO<sub>2</sub> Nanoparticles Addition on Structural, Optical and Dielectric Characteristics of PVA/PVP for Pressure Sensors. Physics and Chemistry of Solid State. 2022;23(2):353-360.
- 45. Abdelhamied MM, Atta A, Abdelreheem AM, Farag ATM, El Okr MM. Synthesis and Optical Properties of PVA/PANI/ Ag Nanocomposite films. Journal of Materials Science: Materials in Electronics. 2020;31(24):22629-22641.
- 46. Elbasiony AM, AbdElrahman M, Said BAM, Abdelhamied MM, Awed AS. Structural and linear/nonlinear optical properties of PVC/ZnFe<sub>2</sub>O<sub>4</sub> nanocomposites for optoelectronic devices. J Thermoplast Compos Mater. 2024;38(5):1927-1949.